Jestr

Journal of Engineering Science and Technology Review 13 (1) (2020) 147 - 159

JOURNAL OF
Engineering Science and Technology Review

Research Article

www.jestr.org

Experimental Study on Bending Behavior and Finite Element Simulation Analysis of Glued Wood Inverted T-beam

Zhenyu Rao, Fan Ning, Junzhu Li, and Jiejun Wang*

School of Civil Engineering, Central South University of Forestry and Technology, Changsha 410004, China

Received 3 December 2019; Accepted 24 February 2020

Abstract

The rectangular section beam of traditional stud-connected glued wood easily causes slip and stress concentration on the joint surface between the bridge deck and the beam. As such, it becomes difficult for the beam and the slab to bear the force together. Moreover, the bearing capacity, rigidity, and integrity of the structure weaken. This study presents the experimental and shear stress calculation models of the T-beam formed by gluing the bridge deck and the rectangular beam together to improve the bearing capacity and rigidity of the structure and the overall mechanical performance of the beam and the slab. Two groups of six parallel glued T-beams were designed and manufactured using Larixgmelinii as raw material. The T-beam was reversed into an inverted T-beam, which was loaded in the middle of the span under the condition of simple support at both ends, so that the rib plate was compressed and the wing plate was tensioned. In this way, the mechanical performance of the negative bending moment of the supporting section of the continuous T-beam was simulated. Results of strain, deflection, flexural rigidity, ultimate bearing capacity, and ductility of the two groups of specimens were measured and analyzed. The failure mode and mechanism of glued wood beam were also observed and evaluated. The glued wood inverted T-beam model was established by the ABAQUS finite element software. Furthermore, the midspan deflection, measuring point displacement, strain, and failure mechanism of the component under the same load level were simulated and investigated, and the test results were verified. Results demonstrate that shear failure occurs along the grain of the beam. In comparison with those of group A, the yield load, yield displacement, ultimate bending capacity, ultimate displacement, flexural rigidity, and ductility coefficient of group B decrease by 9.7%, increase by 27.5%, decrease by 10.4%, increase by 42.7%, decrease by 36%, and increase by 22.4%, respectively. The unfavorable area of the shear stress of the simulated beam under the ultimate load coincides with the position where crack in the test beam developed. The deflection curve of midspan load and the transverse distribution curve of flange strain were in good agreement with each other. The deviation between the simulated and the test values of the midspan deflection and the maximum tensile compression strain did not exceed 15%. The conclusions obtained in this study provide a theoretical reference for further investigation of the mechanical properties of glued wood T-section beams.

Keywords: simply supported inverted T-beam, Glulam continuous T-beam negative Bending Moment, Height Span Ratio and Shear Span Ratio, Bending Capacity, Shear Along Grain

1. Introduction

Timber construction is the essence of Chinese traditional architecture. However, China's forest resource supply was once limited because of excessive logging. Therefore, the state had to restrict the usage of wood in engineering construction, thereby stagnating the development of timber architecture for more than 20 years. At present, "green, healthy, and environmental protection" has become the theme of world development. As a green building material, glulam is a reasonable choice to follow the trend of development [1]. Considering that the strength of wood in traditional wood structure cannot be fully exerted because of the stress concentration caused by defects, such as knots and twills, glued wood is used in the modern wood structure instead of log, thereby compensating the shortcomings of ancient wood structure in terms of span, bearing, and function. After pressure gluing, the wood structure exhibits uniform quality, high strength, and unrestricted component section, thereby extending its use in higher and larger building structures. Glued wood buildings are vigorously investigated and promoted for application with the development of the tourism industry in China, the increasing demand for natural environment and traditional building protection, and with the support of industrial policies.

Despite the high tensile and compressive strength of wood along the grain, its low modulus of elasticity and shear strength resulted in the low bending capacity and rigidity of glued wood rectangular beam, which failed to meet the large span and bearing capacity requirements. However, the traditional glued wood rectangular section beam, the bridge deck, and the rectangular beam are connected by bolts and studs. As such, the joint surface becomes prone to slippage, and the beams and plates experience difficulty in bearing loadings together. This difficulty resulted to problems, such as stress concentration and screw corrosion and loosening and weak structural bearing capacity, stiffness, and integrity. Scholars carried out a large number of studies [2-6] with respect to the mechanical properties of wood and the structural properties of wood beams. However, the actual implementation of these methods is complicated and costly, thereby limiting their application to date. Therefore, the effective improvement of the overall mechanical

*E-mail address: jzgrzy773371@163.com
ISSN: 1791-2377 © 2020 School of Science, IHU. All rights reserved.
doi:10.25103/jestr.131.20

performance, ultimate bearing capacity, and stiffness of the structure while saving cost is still an urgent problem.

Accordingly, this study proposes the gluing of the bridge deck and the rectangular beam to form a T-beam component under common stress and turn the T-beam into an inverted one, which is loaded in the middle of the span under the condition of simple support at both ends. In this way, the rib plate is compressed, and the wing plate is tensioned, thus simulating the mechanical performance of the negative bending moment of the supporting section of the continuous T-beam. This study examines the bending performance of the negative bending moment of the midspan section of the continuous T-beam. The strain, deflection, flexural rigidity, ultimate bearing capacity, ductility results, failure mode, and failure mechanism of the midspan section of the glued timber T-beam are analyzed thoroughly by combining the static load field test, theoretical analysis, and finite element simulation.

2. State of the art

At present, the studies on glued wood structure mainly focus on the enhancement of the mechanical properties of materials, the performance of glued wood beams, and the problems that involve composite components. Frangi.A [2] proposed a bilinear elastic–plastic tension compression constitutive model in terms of the mechanical properties of wood materials, which assumed that the rising section of the compression zone was linear elastic. When the load reached the compressive yield strength, the stress remained unchanged. However, the model ignored the stress–strain change in the compression zone after entering the plastic stage. Robertomasi [23] applied the ultimate strain method based on the simplified bilinear or double broken line constitutive model to analyze the flexural capacity of glued wood beams. Nevertheless, this method failed to consider the elastoplastic characteristics of the compression zone. Given a large number of tests, Norlin [3] introduced the stress–strain relationship, which could truly reflect the tension and compression of wood. Nonetheless, given that the model involved many parameters, its calculation and analysis were rather complicated. Bazan [4] simplified the Blass model and proposed a twofold linear tension compression constitutive model. The model also assumed that the rising section of the compression zone was linear elastic, and the falling section was a straight line with a certain slope, which was consistent with the actual situation. Considering the anisotropic characteristics of wood, Neuhaus [5] investigated the elastic behavior of spruce through tensile and torsional tests using water content as a parameter; however, the plastic stage was not analyzed. Andrew H. B[6] explored the relationship among the bending strength, the axial tensile, and compressive strength of wood. The model of the relationship between the tensile and compressive strength was established, but the anisotropic characteristics of the material were not considered. Melzerová. [7] discussed the influence of the distribution of wood knots on the bending strength of glued wood beams by establishing the finite element model of glued wood beams with knots, but optimization recommendations were not addressed. Istie Rahayu [8] investigated the influence of the single board thickness on the bending strength of laminated veneers. Results showed that the bending strength of mature veneers was 7%–22% higher than that of young veneers, but the influence range of thickness on strength was not indicated.

With regard to wood beam components, Rammer [9] studied the relationship between shear strength and beam size and between shear strength and bending strength and then proposed the empirical formula of shear strength of glued wood rectangular beam. However, the formula was inapplicable to large-scale structures. Cao L et al. [10] collated previous research results, analyzed the influence of shear span ratio, component size, test method, crack, and dry and wet conditions on the shear resistance of glued wood beam. Several theoretical methods for shear design of glued wood beam were also evaluated. However, the exact calculation formula of bearing capacity was not given. In the same year, Hu X F [11] analyzed the carbonization speed, mechanical properties, and fire resistance limit of fired glued wood beams. Moreover, the change rule of fire resistance limit with load ratio and section size was obtained through finite element simulation. However, the anisotropic characteristics of wood were ignored, thereby making the further study of the wood properties in all directions under high temperature necessary. Yang T et al. [12] evaluated the positive bending capacity of glulam T-beam and determined the bending shear failure characteristics and the calculation method of the bearing capacity. However, the reliability of the conclusion must be improved because the number of samples is small.

Scholars carried out studies on the enhancement of the performance of glulam beams and composite members and obtained several achievements to date. Yang H F [13] explored the influence of fiber-reinforced polymer (FRP) on the flexural properties of glulam beams and concluded that FRP could enhance the rigidity and flexural capacities of beams to 1.35 times and 1.82 times, respectively compared with the common components. The calculation formulas for the damage and ultimate loads of the tensile surface layer were also proposed, but the study of other cross-section beams was not involved. Xu Q F [14] Yang X H et al. [15] discussed the glulam beams with steel plates and found that the deformation and bending capacities of the members could be improved by pasting steel plates or adding screws at the bottom of the beams. Moreover, the bearing capacity increases first and then decreases with the increase in the thickness of steel plates. However, no detailed analysis on the effect of the interlayer shear on the flexural performance of glulam beams was identified. Guo N [16] pasted the glued bamboo board at the bottom of the glued wood tensile zone. Experimental research showed that the ultimate load of the beam increased by 16.8%–45.9% when 1–3 layers of glued bamboo boards were observed. Subsequently, the bearing capacity decreased as the number of the layer increased. Although the corresponding calculation formula of bending capacity was proposed, the formula could only be applied to the traditional rectangular section beams, indicating its inapplicability to beams with different section forms. Zhang B [17] studied the wood–concrete composite beams and found that their bending stiffness enhanced with the increase in shear connection degree, but the connection performance between the shear-connecting screws and wooden beams was not investigated. Zhang J [18] arranged parabolic prestressed bars in the beam of glulam in the shape of bending moment diagram of flexural members. Results showed that the curve reinforcement improved the ultimate bearing capacity and bending stiffness of beams more significantly compared with the straight-line reinforcement. Nonetheless, the calculation model of the ultimate bearing

capacity of glued wood beams after reinforcement was not provided.

Therefore, the studies on the bending failure of glued wood beams at home and abroad mainly focused on glued wood materials and various composite members while few studies on the flexural capacity of glued wood beams with different cross-section shapes were existing. Based on the previous study, two groups of glued wood inverted T-section beams with different height span ratios were designed and manufactured at the middle support of the glued wood continuous T-beam through the static load test in the midspan to simulate the negative bending performance to figure out the stress distribution, deformation rule, failure mode, and failure mechanism and to prove the calculation method of bearing capacity. The results of strain, deflection, bending rigidity, ultimate bearing capacity, and ductility of glulam inverted T-beam were measured and analyzed by combining theoretical analysis with finite element simulation. The failure mode and failure mechanism of glued wood beam were observed and analyzed. The theoretical and experimental values of bending shear strength were compared on the basis of the shear strength formula of Rammer. The finite element software ABAQUS was used to establish the model of the glulam inverted T-beam that corresponds to the specimen, and the simulation results were compared with the test data. The research ideas mentioned above are used to further explore the bending characteristics of the negative moment section of the glued wood continuous T-beam span.

The remainder of this study is organized as follows. Section 3 introduces the material property, design dimension, loading device, and measurement scheme of the component; describes the failure mode and failure mechanism of the component; and analyzes the load deflection curve, load strain curve, positive strain transverse distribution curve of the wing plate, and the ultimate bearing capacity in detail. Section 4 presents two groups of glued wood T-beam models established by the ABAQUS software. The deflection, stress–strain cloud diagram, transverse positive strain distribution diagram of flange plate, and shear stress cloud diagram of the model were compared and analyzed. The last section summarizes the whole paper, provides the relevant conclusions, and discusses the problems to be solved in the future.

3. Methodology

3.1 Component materials and design

Two groups of six parallel glued T-beams of Larixgmelini were prepared using polyurethane structural adhesive. The T-beams were formed by gluing wing and rib plates. The size of group A (3 pieces) was 250 × 25 × 21 cm3 (length × width × height) with a depth–span ratio of 1/11 and a shear–span ratio of 5.24, wherein the wing plate was composed of two 3 cm-thick wood plates, and the rib plate was composed of five 3 cm-thick wood plates (Figure 1). The size of group B were 250×25×18 cm3 (length × width × height) with a depth–span ratio of 1/14 and a shear–span ratio of 6.11, where the wing plate was composed of two 3 cm-thick wood plates and the rib plate was composed of four 3 cm-thick wood plates. Only the heights of the two groups' rib plates differ. A diaphragm was added at the bearing and midspan pressure points to avoid local bearing failure. The physical and mechanical properties of Larixgmelinii were measured by the material property experiment. The physical and mechanical properties of polyurethane structural adhesive were provided by Nanjing Tianzhu Science and Technology IndustryCo.,Ltd.(Table1).

Table 1. Physical and mechanical properties of materials

Material	Initial density (g / cm^3)	Moisture content (%)	Tensile strength (MPa)	Compressive strength (MPa)	Bending strength (MPa)	Elastic Modulus (MPa)
Larixgmelin-ii	0.66	14.87	128.68	42.04	86.23	16,900
Polyurethane structural adhesive	1.50	-	≥ 40	≥ 75	-	≥ 3500

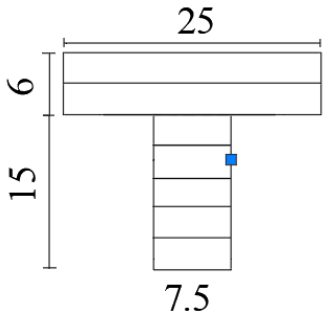

Fig. 1. Cross-section Diagram of 1–3 Specimens (cm)

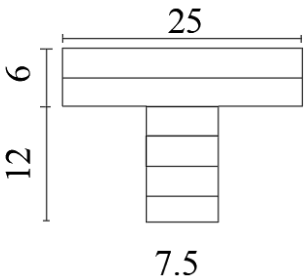

Fig. 2. Cross-section Diagram of 4–6 Specimens (cm)

3.2 Loading and measurement plan

Figure 3 shows the loading arrangement. The T-beam specimen was reversed into an inverted T-beam with the two ends being hinged supports and a single point concentrated load applied in the middle of the span to simulate the negative bending moment and reaction force of the support in the middle of the continuous T-beam span. A 5 cm-thick steel plate was placed at the top of the midspan with a 100 t pressure sensor arranged on the steel plate. Figure 3a shows that the five dial indicators were set at the beam end support and L/2 and midspan position. Six layers of positive strain measuring points were arranged along the height direction of the midspan section of each test piece. Two measuring points were arranged on each layer of the 1st to 5th layers (one on the left and one on the right surface). Five measuring points were arranged on the sixth layer (on the bottom surface of the beam), with a total of 15 positive points. Figures 3b and 3c show the number of strain measuring points. The entire process of the test was controlled by the load when the hierarchical loading method was adopted to mainly test the changes of downward deflection and bending strain of the section, as well as the ultimate bearing capacity of the specimen in the entire

process of the test. The data were collected by the TST3826 static strain test system.

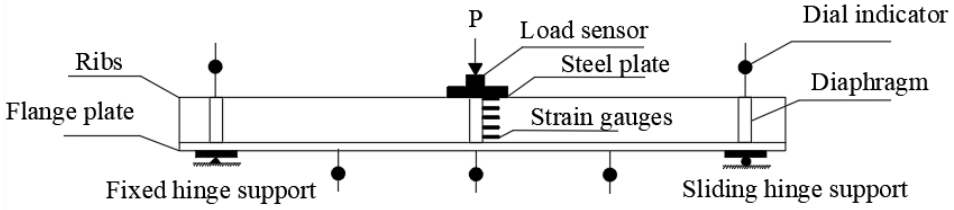

(a)Specimen loading layout (elevation)

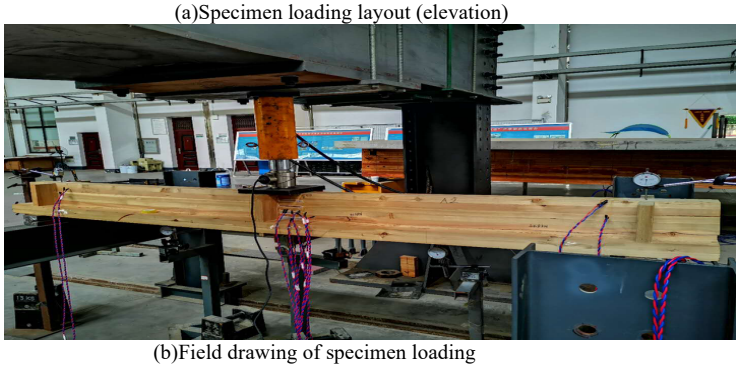

(b)Field drawing of specimen loading

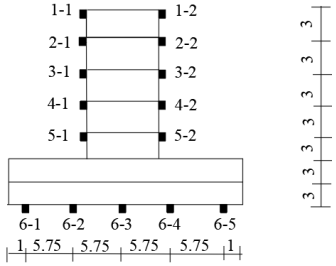

c)Strain measuring points of midspan section of the test piece of Group A (inverted T-beam)

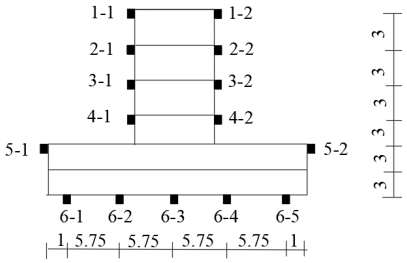

d)Strain measuring points of midspan section of the test piece of Group B (inverted T-beam)

Fig. 3. Test loading and strain measuring point arrangement (cm)

4. Result analysis and discussion

4.1. Failure mode and mechanism analysis

The failure mode of the two groups of test pieces is that the rib plate in the middle of the inverted T-beam section is subject to shear failure along the grain (Figure 4). The inverted T-beam is in the elastic working stage, and the deflection increases smoothly at the initial loading. The wood fiber buckled under compression and the beam cracked internally with a clear sound when the load increased to approximately 65% or more of the ultimate load. The oblique cracks with small angle formed between the surface of the rib and the longitudinal axis of the beam with the increase in the load. A long longitudinal horizontal crack appeared in the middle of the rib and extended to the end of the beam when the ultimate failure load was reached.

According to the *American Code for Wood Construction* ASTM D198, when glulam beams are bent, shear failure generally occurs when the shear span ratio is less than 2.5, shear and bending failure occur when the shear span ratio is greater than 2.5 and less than 6, and bending failure generally occurs when the shear span ratio is greater than 6. The shear span ratios of the test piece Groups A and B are 5.24 and 6.11, respectively. Both test piece groups have shear failure, which is slightly different from the conclusion of the *American Code*.

Mechanism analysis: The failure modes of the two groups of glued wood T-beams include the shear failure along the grain. The tensile strength of the wood along the grain direction is large, the shear strength is small (tensile>bending>compression>shear), the depth–span ratio of the test beam is small, and the shear–span ratio is large. The shear stress ratio near the neutral axis first reaches the shear yield strength with increased load. Moreover, the middle rib plate of the test piece is staggered along the grain and provides a low cracking sound, from which the crack is developed. As the load continues to increase, the wood fiber at the top of the rib plate loses its stability and wrinkles and yields first because the compressive capacity is weaker than the tensile capacity of the wood along the grain. The position of the maximum shear stress moves down simultaneously with the neutral axis. Then, the crack develops rapidly and extends to the beam end, and the specimen is damaged. The main shear crack is located under the neutral axis of the beam and has a small angle with the longitudinal axis. Figure 4g shows that the crack curve is relatively flat.

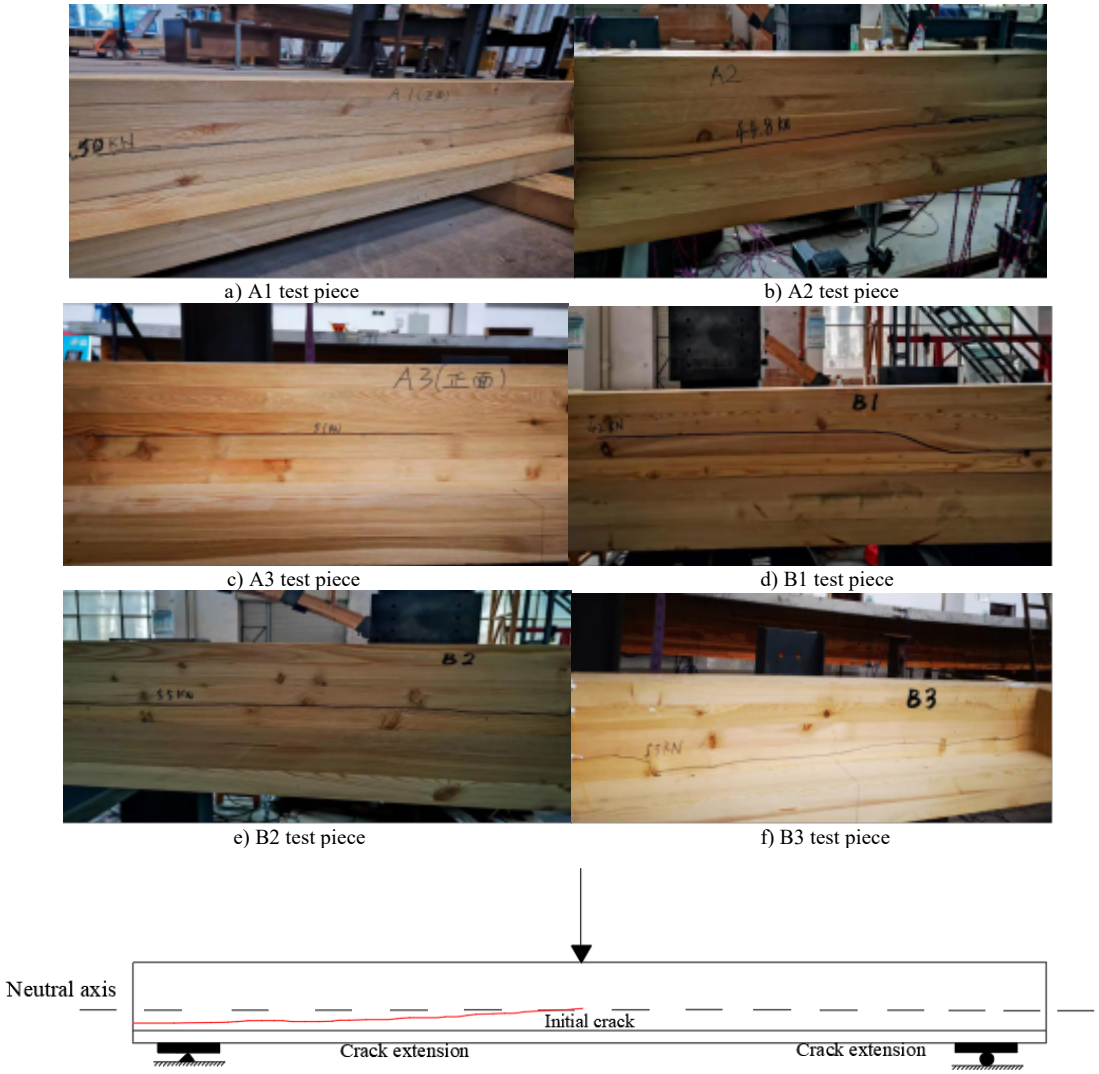

a) A1 test piece
b) A2 test piece
c) A3 test piece
d) B1 test piece
e) B2 test piece
f) B3 test piece
g) Schematic of main cracks during the bending and shearing of glued wood inverted T-beam

Fig. 4. Failure mode of glued wood inverted T-beam

4.2. Load deflection curve

Figure 5 and Tables 2 and 3 show the load midspan deflection curve and mechanical properties of the two groups of specimens.

Figure 5 shows that the specimen underwent elastic stage, elastic-plastic stage, and plastic failure stage during loading. No obvious physical streamline was observed given that the wood is a plastic material. According to the bilinear tension–compression constitutive relation proposed by Banzan [4], the beginning of the compression zone entering the plastic stage was defined as the yield point. The comparison of the load-midspan deflection curves of the two groups of specimens shows that the curve of group A increased linearly before reaching 0.67 pu. The bending stiffness decreased gradually with the increase in load while the deflection increment gradually increased, and the specimen entered elastic–plastic stage until it was destroyed. The elastic properties of the specimen in group B became increasingly evident until it was destroyed with increased load.

It can be concluded by comparing the bending performance of the two groups of specimens in Table 2 that the yield load of group B is reduced by 9.7%, the yield displacement is increased by 27.5%, the ultimate bearing capacity is reduced by 10.4%, the ultimate displacement is increased by 42.7%, and the ductility coefficient is increased by 22.4% compared with those of group A. Hence, the ultimate bearing capacity of the member is reduced, but the ductility coefficient is increased with the increased shear span ratio. Figure 6 shows the comparison of the initial bending stiffness of each test piece considering the secant stiffness at 0–0.4 pu of each test piece as the initial bending stiffness of the test piece [12]. The initial bending stiffness of group A is greater than that of group B.

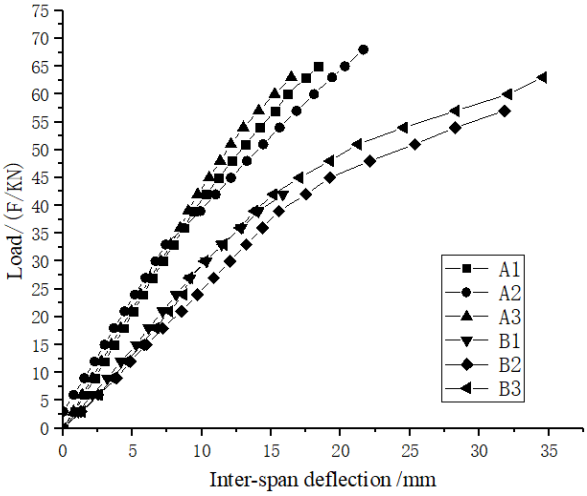

Fig. 5. Load–midspan deflection curve

Table 2. Mechanical properties test data of components

Test piece number	Yield load (KN)	Yield displacement (mm)	Cracking load (KN)	Ultimate load (KN)	Ultimate displacement (mm)	Ductility coefficient $\mu = D_u / D_y$
A1	45	11.23	54	65	18.4	1.64
A2	45	12.1	54	68	21.74	1.79
A3	45	10.53	57	64	16.89	1.33
B1	39	14.09	39	42	15.84	1.12
B2	42	17.5	48	57	31.8	1.82
B3	42	15.15	48	62	34.58	2.28

Table 3. Comparison of test data of two sets of test pieces

Test piece numb-er	Yield load average/KN	Difference ratio/%	Yield displacement average/mm	Difference ratio/%	Ultimate load average/ KN	Differenc-e ratio/%	Average displaceme-nt /mm	Differenc-e ratio/%	Mean coefficient of ductility	Differe-nce ratio/%
Group A	45	-9.7%	11.29	27.5%	65.67	-10.4%	19.01	42.7%	1.59	22.4%
Group B	41		15.58		59.5		33.19		2.05	

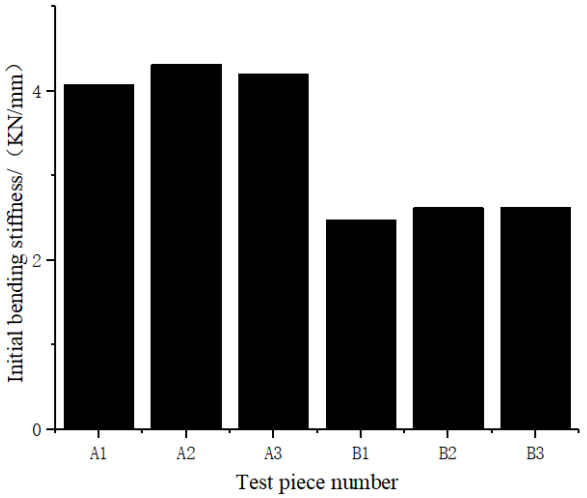

Fig. 6. Initial flexural stiffness

4.3. Load strain curve

Figure 7 shows the change curve of the average positive strain of each measurement point along the height of the midspan section of each group of test pieces with the change in load, wherein measurement point 1 represents the measurement point of the first layer, and the same notations apply hereinafter. Figure 8 shows the distribution of the average strain of the measurement point along the height of the section of each group of test pieces, wherein the vertical and horizontal axes represent the height of the midspan section and the average strain of the measurement point, respectively. The positive and negative signs in the figure indicate tension and compression, respectively.

The strain of the midspan section in the elastic stage during the loading process conformed to the assumption of flat section. Number 1–4 strain measuring points are in the compression area and are negative. Number 5 strain measuring point is in the tension area and is positive. The value of each strain measurement point increased linearly with the load from the initial stage of loading to the failure of the specimen. The tension and compression strains of the timber showed a nonlinear relationship with the change in load when the load exceeded the yield load. The specimen entered the plastic stage. The comparison of the load–strain curves of the two groups of specimens in A and B shows that the compression zone enters the plastic stage first, and the tension zone enters the plastic stage later, indicating that the yield strength of the tensile strength of Xingan larch is higher than that of the compressive strength of Xingan larch. Thus, the tensile performance is not fully developed when the ultimate failure occurs.

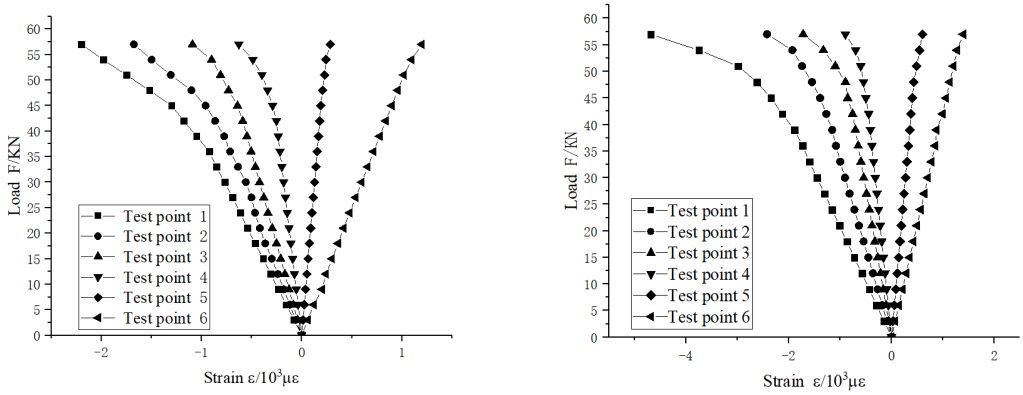

Fig. 7. Load–strain curve

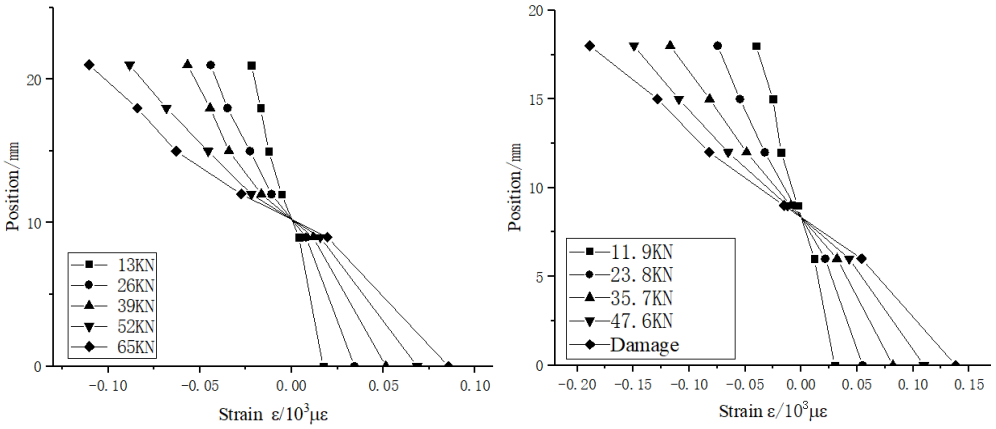

a) Group A test piece b) Group B test piece

Fig. 9. Distribution of strain along the height of the section

4.4. Transverse distribution of positive strain of mid span wing

Five normal strain (longitudinal strain) measurement points were arranged uniformly on the bottom of the wing plate at the midspan section of each test piece. The average values of strain at the measurement points of each group of specimens were taken. Figure 9 shows the transverse distribution of the normal strain of the wing plate under each level of load. The lateral distribution of the positive strain of the wing plate was uneven with a large distribution in the middle and a small distribution at both ends, which were symmetrical. Moreover, the uneven distribution of the strain became more prominent with the increase in the load. Under the maximum load level (54 kn), the lateral distribution of the strain of the wing plate of the two groups of specimens is basically the same. The strain at the center of the wing plate is 10%–13% larger than that at both ends, which is due to the bending shear lag of the beam. Figure 10 shows the distribution of the positive strain of the midspan section of the glulam inverted T-beam.

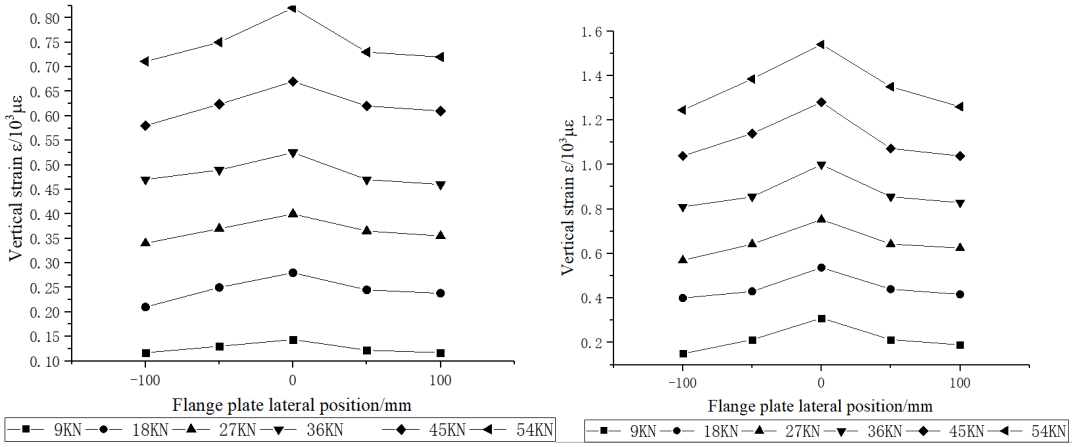

1) Group A 2) Group B

Fig. 9. Lateral distribution of positive strain of wing plate

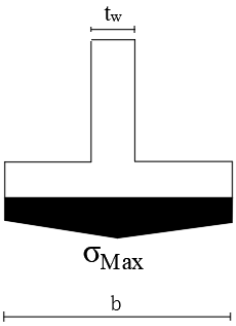

Fig. 10. Nonuniform bending stress distribution diagram considering shear lag effect in the mid-section of inverted T-beam

4.5. Limit state analysis of bearing capacity

The two groups of specimens both have shear failure along the grain, so the shear failure strength is only analyzed theoretically in this test. The maximum shear stress at the central axis of the midspan section of the glulam inverted T-beam under the test load can be calculated according to the formula of material mechanic:

$$\tau_0 = \frac{VS_Z}{bI_z} \quad (1)$$

In the Equation:

τ_0 — shear stress at the central axis of the mid span section of the glued wood inverted T-beam under the test load (N / mm2);

V — the shear force of mid span section of glued wood beam under test load (N);

S_z — the static moment of the cross-section above the shear plane of the member to the neutral axis (mm^3);

b — the width of the central axis of the member section (mm);

I_z — the moment of inertia of full section of member (mm^4).

The ultimate shear strength of glued wood beam decreased with the increased component size; hence, the size effect existed. The Rammer [9] shear strength formula (2) of timber beam is used to calculate the ultimate shear strength of glulam inverted T-beam:

$$\tau = \frac{1.3K_{\mathrm{f}}\tau_{ASTM}}{A^{\frac{1}{5}}} \tag{2}$$

In the Equation:

τ — the shear ultimate strength of glued wood beam;

K_{f} — the adjustment of the stress concentration factor of the actual failure strength of wood, taking 2;

τ_{ASTM} — the shear strength of the wood that is equal to 8.5 MPa;

A — the effective shear area of the inverted T-beam.

The maximum ultimate bearing capacity of each group of test pieces is taken as the calculated shear value (68 KN and 62 KN in groups A and B, respectively). The central axes of the test pieces in both groups are at the rib section (width 75 mm). Table 4 shows the comparison between the maximum test value of shear stress and the theoretical value of shear strength of the midspan section of the glulam inverted T-beam. The effective shear area is calculated by Midas civil computer. The maximum shear stress of the two groups of specimens at the time of failure is consistent with the theoretical value calculated by the Rammer formula, which, at the same time, proves that the Rammer shear strength formula is not only applicable to the calculation of the bending shear strength and the bending shear bearing capacity of the rectangular section beam, but also to that of the inverted T-beam with nonrectangular section.

Table 4. Comparison of experimental values and theoretical values of ultimate bending shear stress of glulam T-beam

Member	Neutral axis height $\bar{y}$ /mm	Effective Shear area A/mm²	Static distance S_z/mm³	Moment of inertia I_z/mm⁴	Theoretical value of shear ultimate strength τ /Mpa	Ultimate shear stress test value/Mpa	Relative error δ/%
Group A	75	15250	6.83×10^5	9.647×10^7	3.22	3.21	-0.3
Group B	63.75	15639	5.07×10^5	6.086×10^7	3.2	3.3	3.1

4.6. Establishment of finite element model of glued wood T-beam

4.6.1. Material parameters

Xingan larch is selected as the raw material for glued wood, wherein the mechanical properties of which are in agreement with the strength of the same combination of glued wood in the Design Standard for Wood Structures (GB 50005-2017 [1820]). The standard value of the flexural strength along the grain is 40 MPa, the standard value of the compressive strength along the grain is 33 MPa, and the standard value of the tensile strength along the grain is 29 MPa. The linear expansion coefficient of the wood is 0.3 × 10–5 ℃. The unit weight is 7.5 KN/m3. The initial density is 0.66 g/cm3. Table 5 shows the other engineering constants.

Table 5. Physical and mechanical properties of materials

Engineering elastic constant	Modulus of elasticity (MPa)			Poisson's ratio						Shear modulus (MPa)		
	E_L	E_R	E_T	V_{LR}	V_{RL}	V_{LT}	V_{TL}	V_{RT}	V_{TR}	G_{LR}	G_{RT}	G_{LT}
Numerical value	16900	1690	845	0.36	0.06	0.48	0.04	0.53	0.05	1268	304	1014

4.6.2. Elastoplastic stage constitutive relationship

The tensile side of the glued wood beam is completely linear elastic through the bending test of glued wood beam. The compression side is elastic-plastic [19]. The stress-strain relationship in the tensile zone of wood is completely elastic and the stress-strain relationship in the elastic stage of the compression zone is linearly increasing in the two kinds of ideal elastic-plastic models of wood proposed by Frangi.A [2] and Bazan I MM[4]. Neely S T assumed that the stress value was constant when the compressive yield strength reached the plastic stage, which was inconsistent with the actual situation. Bazan I MM assumed that the plastic stage curve in the compression zone was decreasing linearly, which fit with the change of the actual compressive stress-strain curve. However, given that the model has many parameters, calculating is not easy. Therefore, the author adopts the ideal elastic-plastic constitutive model of tension and compression [20] (Figure 12). Thus, Formula 3 shows the expression.

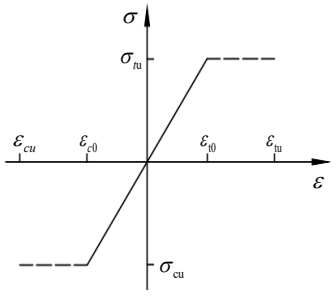

Fig. 12. Ideal elastoplastic constitutive relation

$$\sigma = \begin{cases} E\varepsilon & \varepsilon_{c0} \le \varepsilon \le \varepsilon_{t0} \\ \sigma_{cu} & \varepsilon_{c0} \le \varepsilon \le \varepsilon_{cu} \\ \sigma_{tu} & \varepsilon_{t0} \le \varepsilon \le \varepsilon_{tu} \end{cases} \tag{3}$$

In the Equation:

σ —Stress of the wood;

E—Elastic modulus of wood;

ε —Strain of wood;

σ_{cu} , σ_{tu} — σ_{cu} is the yield compressive stress, and σ_{tu} is the yield tensile stress;

ε_{c0} , ε_{t0} , ε_{cu} , ε_{tu} — Yield compressive, yield tensile, ultimate compressive, and ultimate tensile strains.

4.6.3. Establishment of ABAQUS finite element model

The wood beam is set as X-axis along the grain direction, Z-axis vertically, and Y-axis crosswise using the experimental model to model the size of the beam. The dimension unit is mm. The size of the flange plate is set as 2500×250×30 cm, the size of the rib plate is set as 2500×75×30 cm, the size of steel plate is set as 225×150×15 cm, the wood mass density is 670 g/mm^3, the steel plate mass density is 7850 g/mm^3, the elastic modulus is 2.1×105 MPa, and the Poisson's ratio is 0.3. Table 5 shows the material properties of Larixgmelinii. ABAQUS is used to assign direction of material properties to provide anisotropic properties to each layer. Figure 13 shows that two flange laminates, five rib laminates, and one steel base plate to form the test piece of group A with a component size of 2500×250×210 cm are assembled first. Then, Figure 14 shows that two flange laminates, four rib laminates, and one steel base plate to form the test piece of group B with a component size of 2500×250×180 cm are assembled. The size of the square mesh is 40 mm. The steel plate is placed at the center of the bottom layer of the rib plate. Binding constraints are adopted between the layers. The boundary condition is set as simple support. The steel plate is placed on the top of the middle rib plate of the span, and evenly distributed load is applied.

Fig. 13. Inverted T-beam model of Group A glulam

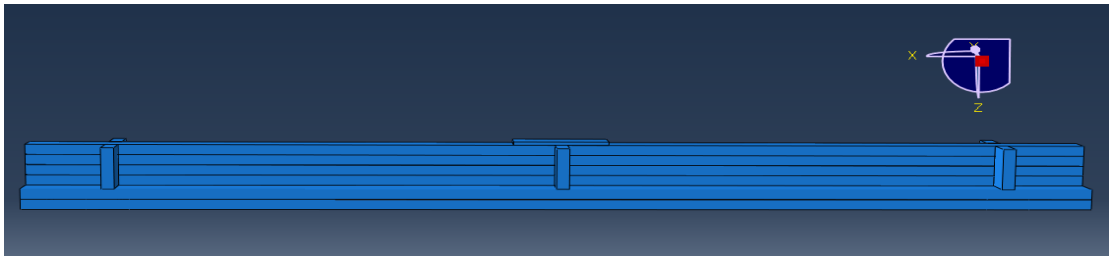

Fig. 14. Inverted T-beam model of Group B glulam

4.6.4. Deformation of glulam inverted T-beam

The A2 and B2 test beams, which have the most representative data to make data comparison with the finite element simulated beams, are considered. The deformation nephogram and load-deflection comparison diagram are presented as in Fig 15.

Figure 15 shows that the bending trend of the two groups of glued wood inverted T-beams is basically the same. The midspan deflection test values of the two groups of specimens are 21.74 mm and 34.58 mm, respectively when the ultimate load is reached (68 KN and 62 KN in groups A and B, respectively). The neutral axis gradually moved down from the rib plate to the flange plate with the increased load. The maximum deformation in the middle of the beam span is not at the bottom of the flange plate according to the finite element simulation. The deformation of each point in the middle section of the two groups of specimens decreased with the increased distance from the vertical neutral axis. The maximum deformation (26.3 mm and 36 mm in groups A and B, respectively) occurred at the neutral axis.

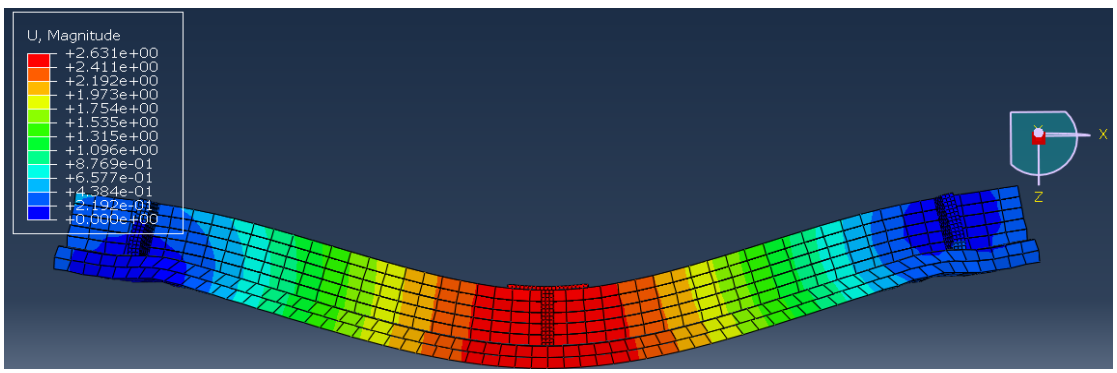

(a)Group A simulated beam

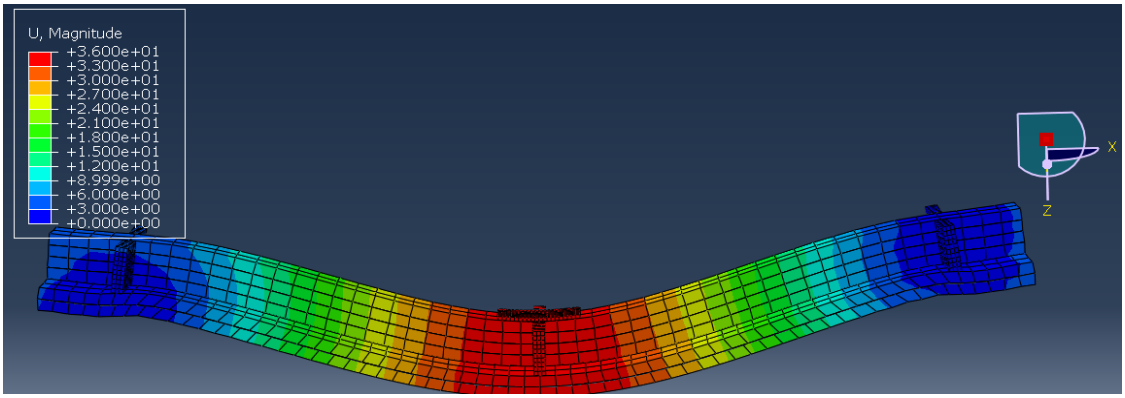

(b)Group B simulated beam

Fig.15. Deformation diagram of glulam inverted T-beam

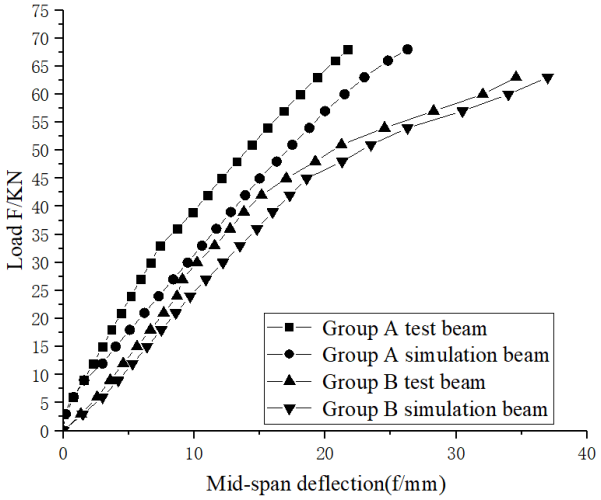

Fig. 16. Comparison of load-span deflection curves between test and simulated beams

Figure 16 shows that the load deflection curves of the test beam are consistent with that of the finite element simulated beam. The analysis results of the two groups of finite elements are larger than the test values. The curve showed a linear relationship at the beginning of loading. When the load reached the yield strength, the specimen entered the yield stage, the curve began to show a nonlinear relationship, and the deflection deformation increased with the increased load until the ultimate strength was reached.

4.6.5. Strain results and failure reasons of glulam inverted T-beam

Given the anisotropic characteristics of wood and the complex nonuniformity of materials, no unified theoretical framework was identified to study the plastic stage of wood beams. In addition, the use of the finite element analysis to determine the failure load and failure mode of wood beams is also misleading and has certain limitations. The failure mode of glued wood beams should be considered from many perspectives, such as stress and strain.

(1)Strain nephogram of glulam inverted T-beam in tension and compression along the grain.

The semistructure is used for analysis based on the symmetry of wood beam. Figures 17 and 18 show the tensile and compression strain nephogram of two groups of finite elements simulated beams along the grain direction.

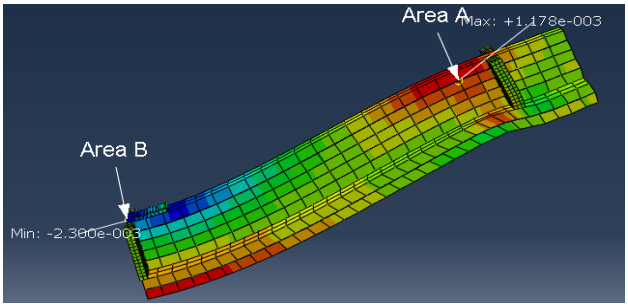

Fig. 17. Tensile and compression strain diagram of group A simulated beam along the grain direction

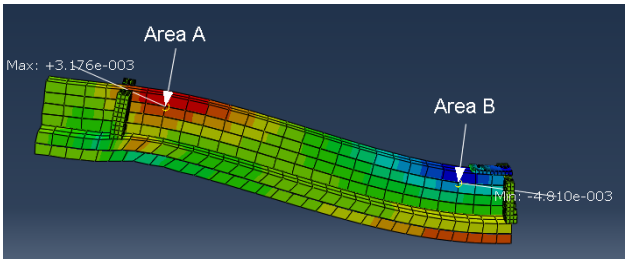

Fig. 18. Tensile and compression strain diagram of group A simulated beam along the grain direction

Two unfavorable areas of tensile and compression strain in the two groups of beams were identified, wherein both were located in the area B of the maximum compression strain at the top of the rib directly below the steel base plate. The area A of the maximum tensile strain at the top of the rib was directly above the hinge support plate. Table 5 shows the maximum tensile and compression strain values.

Table 6. Maximum tensile and compressive strain of glulam inverted T-beam (unit: $\times 10^{-3}\varepsilon$)

Component	A area	B area	Maximum tensile strain zone	Maximum compressive strain zone
Group A	1.178	−2.3	A area	B area
Group B	3.176	−4.81	A area	B area

Table 5 shows that the maximum tensile and compression s-train areas of the two groups of glulam inverted T-beams we-re the same. Thus, the maximum compression strain of both were reached directly below the steel base plate with and $-4.81\times 10^{-3}\varepsilon$,respectively. The maximum tensile strain is reached at the top of the rib plate directly above the hinged suppor-t, which were $1.178\times 10^{-3}\varepsilon$ and $3.176\times 10^{-3}\varepsilon$ .respectively. T-he ultimate

tensile strain of wood is generally 0.005–0.006 ε. The ultimate compressive strain is 0.010–0.012 ε [21]. The size effect existed, which decreased with the increased s-ize of the specimens. The tensile and compression strain of wood fiber at the edge of tension side and compression side of the two groups of finite element simulated beams did not exceed the ultimate tensile and compression strain under the ultimate load. Therefore, no tensile and compression failure were observed, which was consistent with the failure modes of the two groups of members in the test due to the occurrence of shear failure along the grain.

(2) Comparison of test simulation of the transverse distribution of normal strain of midspan wing

Table 3 shows that the yield load of group A was 45 KN, with an average limit load of 65.7KN and the yield load of group B was 42 KN, with an average limit load of 59.5 KN. The load levels of 45 KN and 65 kn were taken to draw the comparison diagram of test simulation of the elastic working stage and the plastic working stage of group A. The load levels of 42 KN and 59 KN were taken to draw the comparison diagram of test simulation of the elastic working stage and the plastic working stage of group B (Figure 19).

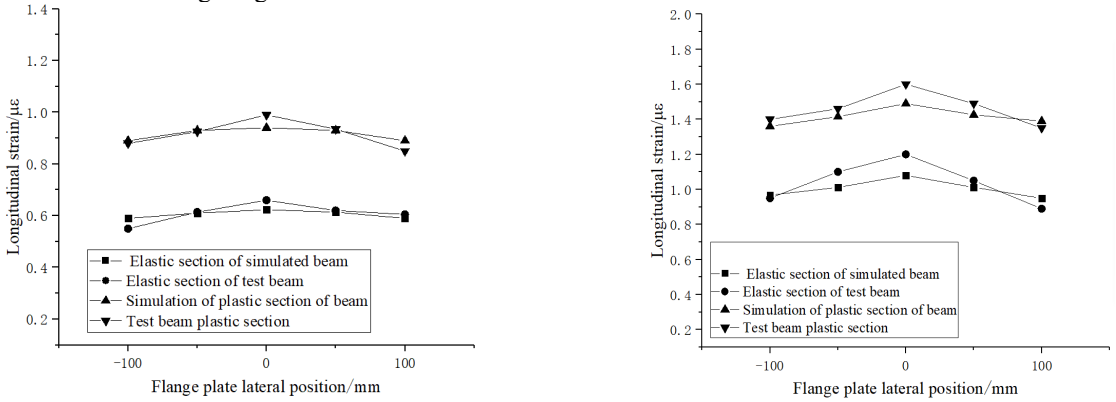

a) Group A test piece b) Group B test piece

Fig. 19. Experimental simulation comparison of lateral strain distribution of wing panel of glulam inverted T-beam

Figure 19 shows that the test values were consistent with the values of the finite element simulation. Given the ideality of the finite element simulated beams, the transverse strain was symmetrical. The transverse strain of the flange decreased with the increased distance to the rib under the influence of shear lag. The maximum deviation of the test value and the simulation value is 6.8%.

(3) Shear nephogram

Shear failure occurred along the grain during the test. Figure 4 shows that shear cracks appeared in the middle of the rib of the two groups of specimens. The top of the rib was not compressed, and the bottom of the flange plate was not pulled. Hence, the shear stress of the glulam inverted T-beam was analyzed further. According to the shear stress reciprocal theorem, S13 and S31 (shear stress τxy along Y in Y-Z plane and shear stress τyx along X in X-Z plane) are equivalent to each other under the influence of vertical load, which is far greater than the shear stress in other directions. Figure 25 shows the spatial stress state of wood beam unit. The shear strength varied significantly in different directions under the influence of the ring area or the shear direction. The shear strength of wood increased with the increased twill angle, wherein the shear strength along the twill (the angle of twill is 0°) is the smallest, and the shear strength of striation (angle of twill is 90°) is maximum. Therefore, studying the shear stress τyx along the grain of wood beam is necessary. Figure 20 shows the shear stress nephogram of glulam inverted T-beam.

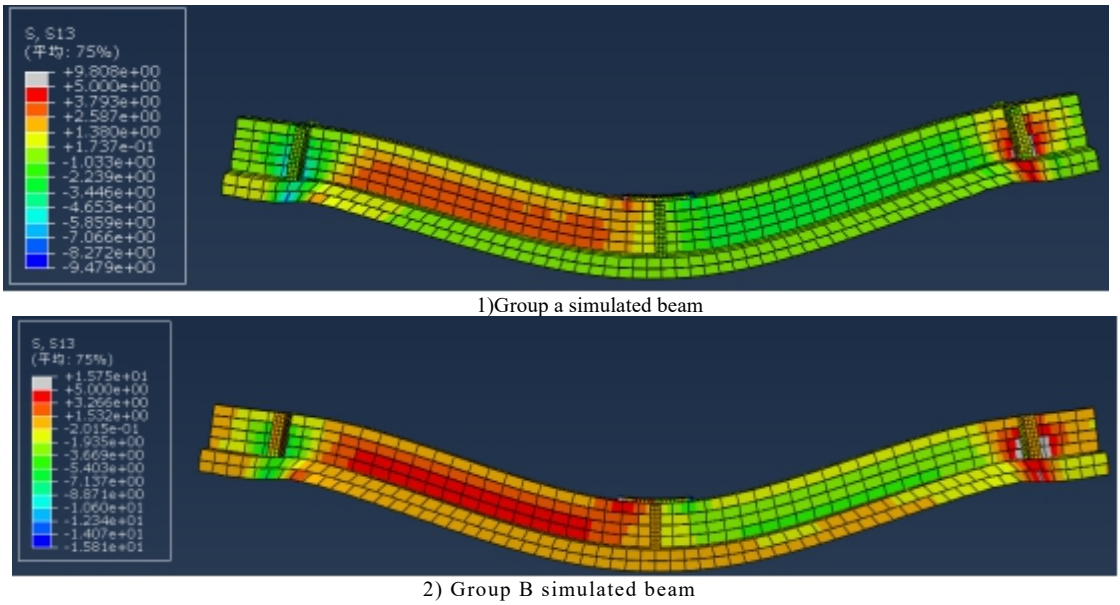

1)Group a simulated beam

2) Group B simulated beam

Fig. 20. Cloud shear stress diagram under the limit load (MPa)

Table 7. Comparison of experimental and finite element results

Componet	Group A beam			Group B beam		
	Test date	Simulation data	Differ	Test date	Simulation data	Differ
Deflection (mm)	21.92	25.54	14%	35.11	37.47	0.9%
Compressive strain $(\times 10^{-3}\varepsilon)$	-2.41	-2.3	4.5%	-5.1	-4.789	1.5%
Maximum strain $(\times 10^{-3}\varepsilon)$	1.205	1.178	2.2%	3.21	3.176	1.05%
Maximum shea-r stress (Mpa)	3.29			3.8		

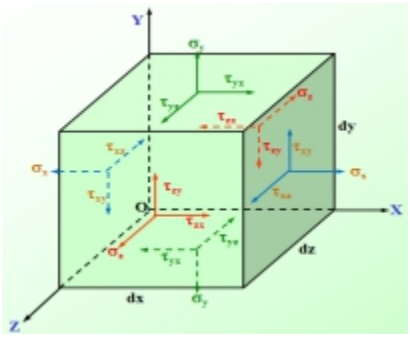

Fig. 21. Schematic of element body spatial stress state

Figure 20 shows that when the two groups of beams bear the ultimate load, the unfavorable area of the shear stress of the glulam inverted T-beam appears at the lower left position of the rib plate, which is consistent with the position of the test beam where crack develops (Figure 4). The maximum shear stress in the unfavorable area of the shear stress is 3.29 MPa and 3.8 MPa in the case of group A and group B beam failure, respectively, which are far greater than the shear strength along the grain of 1.1 MPa of Larixgmelinii [18].

Table 7 shows the comparison of the test results with those of the finite element simulation. The deflection difference between the two groups of specimens under the ultimate load is less than 15%. The difference between the simulation value and the test value of the maximum tensile and compression-n strain of the section is less than 10%. The maximum shear stress is greater than the shear strength along the grain. The unfavorable area of the shear stress is consistent with the position of the test beam where crack develops; hence, the si-mulation results are accurate and reliable.

5. Conclusions

This study proposed the gluing of the flange plate and the web to form a T-section to enhance the ultimate bendingbearing capacity, integrity, and rigidity of glulam beams and to explore the bending characteristics of the negative bending moment of the mid-span section of glulam continuous T-beams. In addition, two sets of simple supported beams with inverted T-shaped cross-sections of glulam with different height-span ratios were designed and manufactured. The beams were loaded in the midspan with simple support at both ends to compress the ribs and exert tension on the wings to simulate the flexural resistance of the negative bending moment of the support section of the continuous T-beam. The strain, deflection, flexural rigidity, ultimate bearing capacity, and ductility of the two groups of test pieces were analyzed through model test and theoretical analysis. Subsequently, the theoretical results were compared with the finite element simulation results. Moreover, the damage morphology and mechanism were observed and analyzed. The conclusions are presented as follows:

(1) Both groups of specimens experienced shear failure. Such outcome was in accordance with the conclusion of ASTM D198 on the relationship between failure mode and shear-span ratio of glulam rectangular beams, but not completely consistent. That is, the failure mode of the T-beam was not completely consistent with that of the rectangular beam.

(2) As the shear–span ratio increased, the ultimate bearing capacity and bending stiffness of the member decreased, but its ductility coefficient increased;

(3) The Rammer shear strength formula was adopted to calculate the flexural shear capacity of the T-beam. The theoretical results were consistent with the test results, indicating that the formula could be applied to the calculation of the ultimate bending-bearing capacity of T-section beam.

In this study, the field experiment, theoretical research, and finite element software simulation were combined to reveal the bending characteristics of the negative bending moment of the midspan section of glulam continuous T-beams, clarify the failure mechanism, analyze the cause of failure, and to propose the calculation formula of the ultimate bearing capacity, which had certain reference significance to the follow-up research. However, the shear lag effect of the T-section beam and the optimal width range of the flange plate cannot be studied effectively because of the small number of specimens and the size problem of the flange plate. Therefore, in-depth research must be conducted in the future.

Acknowledgements

This work was supported by the International S&T Cooperation Program of China (Grant No.2014DFA53120) and the Special Research Program for Public-welfare Forestry of China (Grant No.201304504-3).

This is an Open Access article distributed under the terms of the Creative Commons Attribution License

References

1. Fan, Y. Y., Zhu. Y., "Research Status and Prospects of Glued Wood Structure".*Low Temperature Building Technology*, 39(01), 2017, pp.48-49+55.
2. Frangi, A., König, J., "Effect of increased charring on the narrow side of rectangular timber cross-sections exposed to fire on three or four sides". *Fire and materials*, 35(8), 2011, pp. 593-605.
3. Norlin, L. P., C. M., Norlin., F. Lam., "Shear behaviour of laminated Douglas fir veneer". *Wood science and technology*, 33(03), 1999, pp. 199-208.
4. Malhotra, S. K., Bazan, I. M. M., "Ultimate bending strength theory for timber beams". *Wood science*, 13(01), 1980, pp. 50-63.
5. Neuhaus, H., "Über das elastische Verhalten von Fichtenholz in Abhängigkeit von der Holzfeuchtigkeit". *Holz als Roh-und Werkstoff*, 41(01), 1983,pp. 21-25..
6. Buchanan, A. H., "Bending strength of lumber". *Journal of structural engineering*, 116(5), 1990, pp. 1213-1229.
7. Melzerová, L., P. Kuklík., M. Šejnoha., "Variable local moduli of elasticity as inputs to FEM-based models of beams made from glued laminated timber". *Technische Mechanik. Scientific Journal for Fundamentals and Applications of Engineering Mechanics*, 32(2-5), 2012, pp. 425-434..
8. Rahayu, I., Denaud, L., Ruelle, J., "The effect of juvenility and veneer thickness on bending strength of Douglas-fir laminated veneer lumber". *Journal of the Indian Academy of Wood Science*, 13(01), 2016, pp. 64-72.
9. Rammer, D. R., Soltis, L. A., "Experimental shear strength of Glulam-laminated beams". In: *Forest Products Laboratory, Research Paper: FPL-RP-527*, Madison WI, USA: USDA, 1994, pp. 1-38.
10. Cao, L., Chen, B. W., "Summary of Research on Shear Properties o-f Glued Wood Beams". *Engineering Mechanics*, 35(06), 2018, pp. 1-5+14
11. Hu, X. F., "*Experimental Research on Fire Performance of Glulam Structure Members*". Master thesis of Southeast University, China, 2018, pp.21-39.
12. Yang, T., Wang, J. J., Ning, F., Rao, Z. Y.,"Experimental research o-n flexural bearing capacity of larch glulam T-beam".*Journal of Central South University of Forestry and Technology*, 39(05), 2019, pp. 124-131.
13. Yang, H. F., Liu, W. Q., "Study on flexural behavior of FRP reinforced glulam beams".*Journal of Building Structures*, 28(01), 2007, pp. 64-71.
14. Xu, Q. F., Zhu, L., Chen, J. F., Li, X. M., "Experimental study of timber beams strengthened with steel plates". *Journal of Central South U-niversity:Science and Technology*, 43(03), 2012, pp. 1153-1159.
15. Yang, Y. H., Xue, W., Guo, N., "Bending performance of glued-lum-ber beam reinforced with steel plate".*Journal of JilinUniversity:Engineering Science*, 47(02), 2017, pp. 468-477.
16. Guo, N., Zhang, P. Y., Zuo, W., Zuo, H. L., "Bending performance of glue-lumber beam reinforced by bamboo plyboard".*Journal of Jilin Uni- versity:Engineering Science*, 47(03), 2017, pp. 778-788.
17. Zhang, B., Cao, Y., Huang, T., Zhang, W., Jiang, Y. C., Hu, X. Z., "Experimental study on bending behavior of full-scale glulam-lightweig-ht concrete composite beam".*Journal of Building Structures*, 38(S1), 2017, pp. 297-301
18. Zhang, J., Wang, W. C., Qiu, R. G., Shen, H., Xu, Q. F., Gao, S., "Experimental study on short-term flexural behavior of internal prestres-sed".*China Civil Engineering Journal*, 52(05), 2019, pp. 23-34.
19. Zhou, X. Y., Cao, L., Zeng, D., He, C. H., "Flexural capacity analysi-s of glulam beams". *Architectural structure*, 45 (22), 2015, pp. 91-96
20. Pan, Y., Yuan, S., Wang, H. Q., Wang, X. Y., Lin, Y. J., "Numerical analysis of mechanical behavior of Tou-xin-zao and Ji-xin-zao tou-kun-g in Chinese ancient timber structures". *Civil architecture and environm-ental engineering*, 39 (05), 2017, pp. 9-15
21. Roberto, T., Maria, A. P., Maurizio, P., "Ductile design of gluedlami-nated timber beams". *Practice Periodical on Structural Design and C-onstruction*, 14(3), 2009, pp. 113-122.